Chilean brush tailed mouse (*Octodon degus*): a diurnal precocial rodent as a new model to study visual receptive field properties of superior colliculus neurons

N.I. Márquez[1]* [https://orcid.org/0000-0002-4200-6211], P.F. Fernández-Aburto[2] [https://orcid.org/0000-0002-5695-6234] , A. Deichler[1] [https://orcid.org/0000-0002-2048-8539], I. Perales[1] [https://orcid.org/0009-0006-0394-3049], J.-C. Letelier[1] [https://orcid.org/0000-0001-9484-026X], G. J. Marín[1,3] [https://orcid.org/0000-0003-2961-6469], J. Mpodozis[1†] [https://orcid.org/0000-0003-0786-5579], S.L. Pallas[4†*] [https://orcid.org/0000-0002-1760-7437]

[1]Depto. Biol., Univ. de Chile, Santiago, Chile; [2] Instituto de Ecología y Biodiversidad (IEB), Las Palmeras 3425, Ñuñoa, Santiago, Chile; [3]Facultad de Medicina, Universidad Finis Terrae, Santiago, Chile; [4]Dept. of Biol., Univ. of Massachusetts-Amherst, Amherst, MA; [†]These authors share senior authorship.

Abbreviated title: **Octodon degus superior colliculus receptive field properties**

*Correspondence should be addressed to:
S.L. Pallas
Department of Biology, University of Massachusetts Amherst
221 Morrill Science Center III
611 North Pleasant Street
Amherst, MA 01003 USA
spallas@umass.edu

N.I. Márquez
Departamento de Biología, Facultad de Ciencias, Universidad de Chile
Las Palmeras 3425, Ñuñoa, Santiago de Chile
CHILE
imarquez@uchile.cl

Number of figures: **7**
Number of tables: **1**

Acknowledgements: We would like to thank Solano Henríquez for his valuable assistance.

Conflict of interest: Authors report no conflict of interest.

Funding sources: Support for this work was provided by a National Science Foundation grant (IOS-1656838, IOS-2029980), a DARPA grant (HR0011-18-2-0019, TA2), and UMass startup funds awarded to S.L.P., by a Fondo Nacional de Desarrollo Científico y Tecnológico (FONDECYT) grant to J.M. (FONDECYT 1210069), by a FONDECYT grant to G.M. (FONDECYT 1210169), and by a postdoctoral FONDECYT grant to A.D (FONDECYT 3220871).

ABSTRACT

Lab rodent species used to study the visual system and its development (hamsters, rats, and mice) are nocturnal, altricial, and possess simpler visual systems than carnivores and primates. To widen the spectra of studied species, here we introduce an alternative model, the Chilean degu (*Octodon degus*), a diurnal, precocial Caviomorph rodent with a cone enriched, well-structured retina, and well-developed central visual projections. To assess degu visual physiological properties, we characterized the visual responses and receptive field (RF) properties of isolated neurons in the superficial layers of the superior colliculus (sSC). To facilitate comparison with studies in other rodent species, we used four types of stimuli: (1) a moving white square, (2) sinusoidal gratings, (3) an expanding black circle (looming), and (4) a stationary black circle. We found that as in other mammalian species, RF size increases from superficial to deeper SC layers. Interestingly, compared to other lab rodents, degus have smaller RF sizes, likely indicating higher acuity. sSC neurons displayed spatial frequency tuning to grating stimuli from 0.08 to 0.24 cycles/degree. Additionally, neurons from sSC showed transient ON, OFF, or ON-OFF responses to stationary stimuli but increased their firing rates as a looming object increased in size. Our results suggests that degus have higher visual acuity, higher frequency tuning, and lower contrast sensitivity than commonly used nocturnal lab rodents, positioning degus as a well-suited model for studies of diurnal vision that are more relevant to humans.

INTRODUCTION

In studies of visual processing circuitry, the choice of animal model is often based on tradition or convenience. In contrast, animals that have been chosen for auditory processing research are species that have exceptional auditory processing ability. It could easily be argued that more has been learned about auditory signal processing from studies of bats (Razak 2011; Razak and Fuzessery 2015), owls (DeBello and Knudsen 2004), songbirds (Brainard and Doupe 2013), and chinchillas (Jones *et al.* 2015), than from traditional lab animals. The foundational studies of central visual processing were done largely in cats and monkeys (Hubel and Wiesel 1998), but mice are now the model of choice. Although mouse visual system is similar to that of other mammals in many ways (Huberman and Niell 2011; Garrett *et al.* 2014; Juavinett and Callaway 2015), there are important differences, possibly related to their nocturnal habit and poor eyesight, that have unknown consequences for reaching a general understanding of visual system development and function.

In the Pallas lab, the superior colliculus (SC) and visual cortex (V1) of Syrian hamsters were chosen for studies of visual circuit development, largely because hamsters are born earlier and in larger litters than more typically chosen rodent subjects. As in other mammals studied, receptive fields (RFs) in hamster SC and V1 are large at birth and undergo a postnatal refinement process to reach adult size. It had been assumed, based largely on studies of primary visual cortex (V1) in cats and monkeys (Hensch *et al.* 1998; Espinosa and Stryker 2012), that visual pathway development requires early visual experience during a critical period for maturation but not for maintenance of refined receptive fields and response properties. In contrast, the Pallas lab has found that

90 developmental refinement of receptive fields in SC and V1 occurs normally in dark reared
91 hamsters. Continued visual deprivation in adulthood results in a gradual loss of RF
92 refinement in both SC and V1 of adult hamsters (> postnatal day (P) 60) (Carrasco *et al.*
93 2005; Balmer and Pallas 2015). A brief, late juvenile exposure to light stabilizes receptive
94 field size permanently despite continued visual deprivation, but visual experience after
95 sexual maturity (P 60) has no effect (Carrasco and Pallas 2006; Balmer and Pallas 2015).
96 These results raise the question of whether hamsters are unique or if other rodents, in
97 particular those that are diurnal, would exhibit similar independence from visual
98 stimulation during development.

99 Here we characterize the RF properties of SC neurons in Chilean degus (*Octodon*
100 *degus*), a diurnal, precocial rodent species (Fulk 1976; Reynolds and Wright 1979; Long
101 and Ebensperger 2010) with a cone enriched retina and a well-developed visual system
102 (Vega-Zuniga *et al.* 2013). Unlike typical lab rodent species, degus open their eyes at P1
103 and exhibit visually guided behaviors shortly after birth, exposing their visual system to
104 an early visual experience that could shape its maturation. Our results show that degus
105 have clear diurnal characteristics and a better visual acuity in comparison to nocturnal lab
106 rodents. Here we argue that degus are a promising model to study the role of visual
107 experience in the maturation of the visual system and thus might be better suited to model
108 the human visual system.

109

110 **METHODS**

111 **Animals**

112 A total of 10 animals from our colony were used in this study. Animals were housed in
113 metal cages (50 x 40 x 35 cm) with wood shavings as previously described by Márquez
114 *et al.* (2015) in a climate-controlled room under a 12:12 photoperiod in groups of 3-4
115 degus of the same sex. They were fed with rodent-chow Prolab® RMH 3000 (Purina
116 LabDiet®, Inc.), Mazuri chinchilla diet (Mazuri® Exotic Animal Nutrition) and provided with
117 water *ad libitum*. All animal procedures were approved by the *Comité Institucional de*
118 *Cuidado y Uso Animal* (CICUA) of the University of Chile and the IACUC of the University
119 of Massachusetts-Amherst and followed the National Institutes of Health (NIH) Guide for
120 the Care and Use of Laboratory Animals. All procedures met additional standards of care
121 established by SfN and IBRO.

122

123 **Histology and neuronal tracers**

124 Some degus (n=2) were used only for neuroanatomical data collection. The labeling of
125 retinal projections to the SC was performed under gaseous anesthesia using isoflurane
126 (4% in medical oxygen at a flow rate of 100 cc/kg/min) complemented with diazepam (5
127 mg/kg) administrated IP. A glass pipette (tip diameter 15–20 μm) containing 1% cholera
128 toxin subunit B (CTB, List Biological Laboratories, Campbell, CA) in 0.1 M phosphate
129 buffer was injected intraocularly. After 5–7 days survival, the degus were sedated with
130 gaseous isoflurane, placed in a deep state of anesthesia with ketamine/xylazine
131 (ketamine 40-80 mg/kg, xylazine 5-10 mg/kg), and perfused intracardially by passing 200
132 ml of warm saline solution (0.9% in 0.1 M PB) followed by 200 ml of cold
133 paraformaldehyde (PFA, 4% in 0.1 M PBS). The brains were extracted and postfixed
134 overnight in 4% PFA at 4°C, and then transferred to 30% sucrose solution in 0.1 M PB

135 until they sank, for cryoprotection. Brains were sectioned (60 μm), and a CTB
136 immunoreaction assay was performed as described by Deichler *et al.* (2019).

137 For histological confirmation of electrode positioning during electrophysiological
138 recording degus were given an overdose of urethane (3 mg/kg, IP) and perfused
139 intracardially as described above. The brains were postfixed overnight in 4% PFA at 4°C
140 and then transferred to 30% sucrose for cryoprotection. Finally, brains were sectioned
141 (60 μm), mounted, and Nissl-stained (cresyl violet, Merck, Darmstadt, Germany).
142 Reconstruction of electrode penetrations in several experiments verified that our
143 recordings were taken at intervals of 100 microns through a transect passing across
144 layers of the SC, from the SGS into the SGI.

145

146 ***In vivo* recordings**

147 *Animal Preparation.* Pre-op: Degus store wood shavings in their cheeks (Deichler,
148 pers. comm.). Thus, to avoid aspiration of the shavings during anesthesia, they were
149 taken from their cages and placed in a clean cage with paper towels the night before the
150 experiment. Degus (n = 8) were fasted overnight after receiving Dexamethasone (1
151 mg/kg, SQ) to prevent cerebral edema. The morning of surgery, a second dose of
152 Dexamethasone (1 mg/kg, SQ) was given along with atropine (0.1 mg/kg, SQ) to
153 counteract bradycardia and apnea and to reduce mucosal secretions.

154 *Surgery*. Isoflurane (4% in medical oxygen at a flow rate of 100 cc/kg/min) was used
155 for anesthesia induction, then diazepam (5 mg/kg) was administrated IP to induce
156 sedation before degus were anesthetized using urethane (1.25 mg/kg, IP). If necessary,

157 Doxapram was used (2 mg/kg SQ or sublingual) to stimulate respiration. Body
158 temperature was kept between 36 °C and 37 °C throughout the experiment by using a
159 thermo-regulated blanket (FHC, Inc.). To prevent asphyxia due to accumulation of
160 bronchial secretions, degus were tracheostomized after the site was prepped by shaving
161 the neck and chest, cleaning the area with ethanol and povidone, and inserting a tracheal
162 tube. The scalp was shaved, and the head stabilized in a stereotaxic head holder. Then,
163 the surgical site was cleaned with ethanol and povidone followed by a midline incision in
164 the scalp. The muscles and periosteum overlying the skull were retracted, and a small
165 craniotomy above the SC region was made with a surgical micro-drill. After unilaterally
166 aspirating the cortex to expose the SC and covering the site with saline,
167 electrophysiological recordings were obtained by using Epoxy-insulated tungsten
168 microelectrodes (1–2 MOhms; FHC, Inc.) or a 16 Channel multi- electrode array (MEA)
169 (~1 MOhm; Microprobes for Life Science, Inc.) and a multichannel differential amplifier
170 (Model 3600; AM Systems Inc.). A silver chloride wire was implanted in between the
171 exposed bone and muscle as a reference electrode. Physiological data were sampled
172 just before, during, and just after the stimulation at 10-20 kHz, with a band-pass of 3 Hz
173 to 10 kHz, by using a standard PC with a 16-channel A/D converter board (National
174 Instruments Corp). Data acquisition and offline analysis were performed using Igor Pro-8
175 (WaveMetrics, Inc.) or MATLAB (MathWorks, Inc) software.

176

177 **Visual stimulation**

178 Visual stimuli were presented on an LCD monitor (Alienware 25 AW2518HF, 1920 x 1080
179 pixels, 60 Hz refresh rate) placed 32 cm from the degu's eye. Stimulus parameters were

180 controlled with a lab-designed program using the Python (Python Software Foundation) -
181 based open-source application PsychoPy (v.3.1.3). A photodiode that detected the
182 stimulus produced a 5-volt TTL signal that was recorded by the amplifier and used to
183 synchronize stimuli and neural responses. Four types of visual stimuli were used:

184 *Drifting squares.* A white square (~3° diameter) on a dark background was swept from
185 the top to the bottom of the monitor over 4 s, with 1 s intervals between successive stimuli.
186 The position of the square changed in an orderly manner along the horizontal axis of the
187 screen at each sweep, covering the entire screen within 64 runs (**Fig. 1A**). The stimulation
188 protocol was repeated 3 times for each recording location/depth.

189 *Drifting gratings.* Stimuli consisted of full-field, vertical, sinusoidal gratings drifting from
190 temporal to nasal on the LCD monitor. Frequency, contrast and temporal frequency
191 parameters were chosen as in Niell and Stryker (2008). The sinusoidal gratings were
192 presented over 4 s with a 2 s interstimulus interval at a constant temporal frequency (1.5
193 Hz). All combinations of spatial frequency (0.01, 0.02, 0.04, 0.08, 0.16, 0.32 cycles/deg)
194 and contrast (0.0625, 0.125, 0.25, 0.5, 0.75, 1) were presented in a pseudo-random
195 manner. The stimulation protocol was repeated 5 times for each recording location/depth.

196 *Dark looming object.* We presented a looming object consisting of a small, black circle
197 (2° diameter) on a gray background, expanding to 20° in diameter over 250 ms, followed
198 by a 250 ms presentation at its maximum size (Yilmaz and Meister 2013).

199 *Dark static object.* As a control for the looming experiment, we presented a 20°
200 diameter static black circle on a gray background for 500 ms. The looming and static
201 object stimuli were both presented 15 times with 2 s inter-stimulus intervals.

Data processing

The data were band pass filtered (400 to 5000 Hz) by applying a Finite Impulse Response (FIR) filter with a Hamming window (Choi *et al.* 2006). The background noise was estimated using an adaptive filter algorithm (Biffi *et al.* 2010). Events that crossed a threshold of 3.8 times the background noise were considered as spikes. Spikes were sorted into clusters using the discrete wavelet transform for feature extraction, and coefficients were selected to maximize the clusters' distance (Letelier and Weber 2000). The clustering of single units was performed using a *k*-means algorithm with optimal *k*-values obtained by the silhouette cluster analysis (Rousseeuw 1987) (see **Fig. 1B-C**).

Characterization of receptive field properties

Receptive field size

The RF area was assessed for each single unit by binning the data into 100 ms intervals, subtracting the spontaneous firing rate, and fitting a two-dimensional (2D) Gaussian curve to the average of the firing rate across trials:

$$fit = z_0 + Ae^{\left(\frac{1}{2(1-cor^2)}\right)\left[\left(\frac{x-x0}{xWidth}\right)^2 + \left(\frac{y-y0}{yWidth}\right)^2 - \left(\frac{2cor(x-x0)(y-y0)}{xWidth \cdot yWidth}\right)\right]} \qquad (1)$$

where z_0 is the matrix baseline (minimum value of firing rate after the subtraction of the spontaneous firing rate), A is the maximal response amplitude, x_0 and y_0 are the horizontal

222 and vertical positions of the RF's center, *xWidth* and *yWidth* are the radii of the RF, and
223 *cor* is the correlation coefficient between two correlated Gaussian random variables. The
224 RF areas obtained for each single unit were subsequently categorized into depth ranges,
225 using the ranges defined in Table 1.

226

227 *Spatial frequency tuning and contrast responses*

228 Single unit responses were binned in 100 ms intervals and spontaneous firing rate was
229 subtracted. Spontaneous firing rate was obtained from one second interstimulus intervals
230 ranging from 0.5 -1.5 s after each stimulus presentation. Units considered in the analysis
231 showed a mean evoked firing rate $\geq$ 3 Hz after the spontaneous firing rate subtraction.
232 Tuning curves for spatial frequency (SF) were built using mean SF responses at the
233 contrast where the maximum response was evoked, and by fitting the data using a single
234 Gaussian function:

235 $$\mathrm{R}(sf) = R_b + \mathrm{A}e^{\frac{(-sf - x_0)^2}{2\sigma^2}} \qquad (2)$$

236 where R_b is the baseline of the curve, A is the response's amplitude, x_0 is the position of
237 the center of the peak, and σ is the standard deviation. All variables were optimized by
238 finding the minimum of the unconstrained multivariable function using a derivative-free
239 method from MATLAB- fminsearch (Hendrikje *et al.* 2013; Camillo *et al.* 2020). Neurons
240 with $R^2 \leq 0.7$ in the Gaussian fitting function were not considered further for analysis. The
241 values for preferred spatial frequency were obtained from each single unit and were
242 classified as low-pass, band-pass or high-pass according to the specific spatial frequency
243 tuning they displayed. *Low-pass neurons* responded to low spatial frequencies (i.e., 0.01

244 cpd) with a peak firing rate larger than half of the peak's activity amplitude and showed
245 smaller (less than half of the peak's amplitude) or non-responses to higher spatial
246 frequencies. *Band-pass neurons* showed a bell shape response with a maximum at its
247 preferred SF while having low firing rates (lower than half of the peak's response
248 amplitude) for low *sf* (low cut-off) and for high SF (high cut-off). Finally, *high-pass neurons*
249 responded to higher spatial frequencies with firing rates larger than half of the peak
250 response (i.e., > 0.24 cpd). For those neurons showing a band-pass curve we calculated
251 the $\log_2$ bandwidth (high cut-off frequency/low cut-off frequency) to determine how narrow
252 or wide their tuning was (Heimel *et al.* 2005). We also evaluated the linearity of the
253 responses to the drifting grating stimuli at the preferred spatial frequency by calculating
254 the F1/F0 ratio, with F0 being the mean response and F1 the response modulation at the
255 drifting frequency. Both values were calculated by applying the discrete Fourier
256 transformation (Niell and Stryker 2008; Wang *et al.* 2010). Cells showing a F1/F0 $\geq$ 1
257 were classified as linear or simple, whereas those showing a F1/F0 < 1 were classified
258 as non-linear or complex. Single unit responses to different contrasts were obtained by
259 using the spatial frequency value exhibiting the maximum response. The mean responses
260 were fitted using a Naka-Rushton function (Naka and Rushton 1966):

261 $$R(C) = R_b + \frac{gC^n}{S^n + C^n} \qquad (3)$$

262 where R_b is the baseline of the curve, g the gain, S the contrast value at the mid saturation
263 point, n the exponent, and C the contrast. From the fitted curve we obtained: i) the contrast
264 value at half the peak response (C_{50}), which is a measure of contrast response linearity
265 (Heimel *et al.* 2005) and ii) the maximum slope of the fitted curve (maximum rate minus

266 the normalized spontaneous rate), which is a measure for non-linear responses to
267 contrast (Heimel *et al.* 2005).

268

269 *Responses to dark looming objects.*

270 Single unit responses to looming and static objects were binned in 10 ms intervals before,
271 during, and after the stimulus presentation. We calculated the neuronal response by first
272 obtaining the spontaneous firing rate for the 300 ms before the stimulus presentation,
273 then we averaged the responses of the 15 repetitions of each kind of stimulus (looming
274 and static objects) and subtracted the spontaneous firing rate. Raster-plots, however,
275 represent the response of a neuron (firing rate minus the spontaneous firing rate) for each
276 trial. To assess the onset time (latency) and peak response time to the object
277 presentation, z-scores were calculated for each bin taking 300 ms before and 500 ms
278 after each stimulus presented ($t_{stim} = 0$). To ensure the specific response to our visual
279 stimulation we chose a strict threshold; only neurons with a maximum response $\geq$ 5 z-
280 scores were considered in the analysis. The onset time of the response was the first bin
281 at which the response exceeded 2 z-score values and continued increasing until it
282 reached the peak response. The peak time corresponds to the time of the maximal
283 response between the onset of the stimulus and 250 ms (time for the looming object to
284 reach maximum size).

285

286 **RESULTS**

287 **Cytoarchitecture of the SC**

288 The mammalian superior colliculus is a laminar structure composed of 7 main layers,
289 namely, stratum zonale (SZ), stratum griseum superficiale (SGS), stratum opticum (SO),
290 stratum griseum intermediale (SGI), stratum album intermedium, (SAI) stratum griseum
291 profundus (SGP) and stratum album profundus (SAP). This latter layer separates the
292 SGC from the underlying periaqueductal grey (PAG). In agreement with previous findings
293 (Vega-Zuniga et al., 2014; Deichler et al., 2019), we found that SC in degus is a large
294 and highly differentiated structure, in which all layers are well-defined and readily
295 identifiable in Nissl preparations (**Fig. 2A, A'**). As in other mammals (e.g., mouse (Basso
296 and May 2017; Ito and Feldheim 2018), cat (May 2006), tree shrew (Albano *et al.* 1979)
297 and Galago (Balaram *et al.* 2011), but see Major *et al.* (2003)), the SGS in degus appears
298 to contain two subdivisions, upper (uSGS) and deep (dSGS), the former being composed
299 of smaller and less densely packed cells than the latter. Another striking feature is that
300 the SGI in degus appears composed of three subdivisions- upper (uSGI), intermediate
301 (iSGI) and deep (dSGI)- that are readily distinguishable by their differences in cellular
302 density (**Fig. 2A)**, these subdivisions have also been also observed in rats and mice
303 (Wiener 1986; Helms *et al.* 2004).

304 To determine the extent of retinal innervation of SC, we made retinal CTB injections
305 into the vitreous humor. We found that the SC is the largest and most densely innervated
306 retinal target in the degus visual system (**Fig. 2B**). Retinal projections to the degu SC
307 originate almost exclusively from the contralateral eye (Vega-Zuniga *et al.* 2013, 2014;
308 Deichler *et al.* 2020) and thus we did not quantify the ipsilateral projections. The
309 contralateral retinal projections enter the SC through the SO and terminate very densely
310 in the SZ and in both SGS subdivisions, and more sparsely in the SO. However, the

311 dorsal portion of the SO receives denser terminal arborizations than its ventral part (**Fig.**
312 **2B, 2B'**). Retinal projections were not present in the deeper layers of the SC, SGI, and
313 SGP.

314

315 **Receptive field properties in the degu's SC**

316 To characterize the RF properties in the Chilean degu (*Octodon degus*), we presented
317 different visual stimuli, as detailed in the methods section. Our main objective was to
318 characterize the RF properties within the retino-recipient layers, specifically the SGS and
319 SO, that are part of the superficial SC (sSC). Additionally, we assessed whether neurons
320 in the degu's SC exhibited the canonical organization of visual RFs characterized by
321 smaller RF sizes in more superficial layers compared to deeper layers, including the SGI.

322

323 *Receptive field size and shape vary with depth in SC*

324 As a first step to characterize the RF properties of SC neurons in degus, and to compare
325 our findings with previous work in hamsters (Carrasco *et al.* 2005) and mice (Fernández-
326 Aburto *et al*., in prep), we recorded from neurons with RFs located in the frontal visual
327 field, and determined how their size and shape varied across the different SC layers (from
328 SGS to SGI). Illustrations of the size and shape of receptive fields for two single units
329 recorded from the SGS and SGI, respectively, are presented in Figures **3A** and **3B**.
330 Consistent with previous findings, degus showed the canonical organization of visual RFs
331 in the SC (Humphrey 1968), with RF sizes of single units increasing significantly with
332 depth from the SGS to the SGI layer (ANOVA $F_{[6,32]}$: 5.58, p = 0.00048; **Fig. 3C**). The

333 Tukey HSD (honestly significant difference) post-hoc test revealed that the RF areas of
334 single units recorded from the SGI depth range **7** (see **Table 1**) were significantly larger
335 than RF areas of single units from the SGS depth range **1** (p = 0.0006) and significantly
336 larger than RF areas recorded from units in the SGS depth range **2** (p = 0.003). RF areas
337 of single units from SGI depth range **7** were also significantly larger than RF areas of the
338 upper SO depth range **3** (p = 0.003; **Fig.3C**). In addition, we compared RF sizes between
339 the SC layers combined (SGS, SO and SGI), and found a significant difference (ANOVA
340 $F_{[2,36]}$: 12.46, $p < 0.0001$; **Fig. 3D).** RF areas from SGI neurons (area size range: 42.84-
341 162.8 deg^2) were significantly larger (Tukey HSD, p = 0.0001) than RF areas from SGS
342 neurons (area range: 19.8 – 90.97 deg^2), and significantly larger (Tukey HSD, p = 0.0018)
343 than RF areas from SO neurons (area range: 30.35 – 86.01 deg^2). RF sizes from SGS
344 neurons and SO neurons were similar (Tukey HSD test, p = 0.36).

345 Studies on rat and monkey SC have shown that there is a change in RF shape
346 across SC layers, going from near circular RFs in the superficial layers to RFs elongated
347 along the horizontal axis in the deeper layers (Humphrey 1968). To investigate whether
348 degus also exhibit an alteration in receptive RF shape (i.e., circular vs. oval shape), we
349 compared the ratio between the horizontal and vertical axes of the RFs across the SC
350 depth ranges. A ratio close to 1 indicates a symmetrical RF with a circular shape, whereas
351 deviations from this value indicate an elongation of the horizontal axis. Similar to the
352 findings reported by Humphrey (1968), RF symmetry changes significantly between depth
353 ranges; RFs from deeper layers are more elongated along the horizontal axis than RFs
354 from upper layers (ANOVA $F_{[6,32]}$: 4.04, p = 0.004; **Fig. 3E**). The RFs of neurons from SGI
355 depth range **7** were more elongated along the horizontal axis (i.e., asymmetrical) than the

356 circular RF shape of neurons from SGS depth range **1** (p = 0.004) and were also more
357 elongated than the RF shape of neurons recorded from the SGS depth range **2** (p = 0.01).
358 Likewise, neurons from SO depth range **3** showed RF shapes that are significantly more
359 circular than the elongated RF shapes of neurons from SGI depth range **7** (p = 0.037;
360 **Fig. 3E**). Comparisons focusing on the differences between SC layers as a whole rather
361 than the depth level confirmed that as recordings sampled the lower layers, RFs shapes
362 became more elongated along the horizontal axis (ANOVA $F_{[2,36]}$: 6.69, p = 0.003; **Fig.**
363 **3F**). The RFs of SGS neurons were significantly more symmetric (i.e., circular) than RFs
364 of SGI neurons (Tukey HSD, p = 0.002). The shape of the RFs from SO neurons was
365 statistically the same as the RF shape of single units from the SGS and SGI, suggesting
366 a tendency of SO neurons to have elongated RFs.

367

368 *Spatial frequency tuning*

369 Sinusoidal gratings of different spatial frequencies (SF) and contrasts (**Fig. 4A**) have
370 been widely used to characterize RF properties of different visual brain structures in
371 several animal species (Jassik-Gerschenfeld and Hardy 1979; Issa *et al.* 2000; Heimel *et*
372 *al.* 2005). In the case of degus, we found that 47% (228/485) of SGS neurons that were
373 recorded responded to sinusoidal grating stimuli. Of those, 58.3% (133/228) were tuned
374 to specific combinations of SF and contrast (see below). According to their spatial
375 frequency tuning, we classified neurons as low-pass, band-pass or high-pass (see
376 Methods). Most SC neurons were band-pass (60.9%), or low pass (36.8 %); only a few
377 were classified as high-pass neurons (2.3%; see Figures **4B** through **4E'**). Even though
378 the median value of SF preference across all three cell types (low-pass, band-pass and

379 high-pass) was 0.04 cycles per degree (cpd), we found a subset of band-pass neurons
380 (18%) tuned to a higher SF (0.24 cpd) (**Fig. 4F**).

381 To further assess the specificity of SF tuning in band-pass neurons, we quantified the
382 tuning curves' bandwidths (the range of SF to which a band-pass neuron responds).
383 Interestingly, 41% of band-pass neurons were tuned to their preferred SF, with
384 bandwidths ranging between 0.5 and 2.0 octaves (**Fig. 4G**). Additionally, we assessed
385 the extent to which spatial frequency modulates the activity of degus' SC units by
386 calculating the linearity index *F1/F0* (where *F1* is the modulation of the response (firing
387 rate) at the drift frequency of the stimulus, and *F0* is the average firing rate of the
388 response, see Methods) (De Valois *et al.* 1982). We found that most SGS neurons (86%)
389 responded non-linearly to their preferred SF (*F1/F0* < 1) **(Fig. 4H)**, and the rest (14%)
390 responded linearly (*F1/F0 > 1*) (**Fig. 4I)**. The distributions of linear/non-linear responses
391 for the neuronal population is shown in Figure **4J**.

392

393 *Contrast tuning*

394 Overall, SGS neurons increased their response levels with increased contrast. However,
395 there were neurons that showed a linear response to contrast without saturating their
396 response (53.3%; **Fig. 5A**), and others (46.7%) that exhibited different degrees of
397 saturation at higher contrast (**Fig. 5B-C**). Interestingly, such saturating responses are
398 characterized by high contrast gain at low contrasts and low contrast gain at high
399 contrasts (Alitto *et al.* 2019). We further characterized linear and saturating responses by
400 quantifying the contrast at half of the maximum response (C_{50} value) and the relative

401 maximum gain (RMG), i.e., the maximum slope of the normalized contrast response
402 curves (Heimel *et al.* 2005). At the population level, 50% of the neurons showed that the
403 contrast at half of the maximum response (C_{50} value) was 48%, indicating a linear
404 response to contrast (**Fig. 5D**). On the other hand, neurons that show saturating
405 responses can have high (C_{50} < 30, 36% of neurons) or moderate (C_{50} between 30 and
406 40, 17% of neurons) saturation of their responses to contrast. Additionally, the median
407 value of RMG was 1.47 (**Fig. 5E**), indicating slight non-linearity, compared to non-linear
408 responses to contrast in the squirrel's V1 with a median RMG value of 2.8 (Heimel *et al.*
409 2005) . Only 22/135 neurons (16.3%) had a RMG of approximately 1 (between 0.8 and
410 1.4) that we considered as a linear behavior, whereas 28/135 showed RMG values $\geq$ 3
411 (20.7%) and were thus considered non-linear. Interestingly, 50% of neurons (170/477)
412 showed RMG values between 1.4 and 1.5, which we interpreted as weak non-linear
413 responses. Although both measures, C_{50} and RMG, are indicators of linearity, the RMG
414 is less dependent on the fitting process (Heimel *et al.* 2005). Still, both measures suggest
415 that the degus SGS has neuron types that respond in a linear and a nonlinear fashion.

416

417 *SGS neurons respond in a continuously increasing way to looming*

418 To evaluate the units' responses to looming stimuli, we presented 15 repetitions of a dark
419 disc that increased in size from 2 to 20 deg in 250 ms and stayed ON for another 250 ms.
420 As a control we presented a static dark disc (20°) for 500 ms to address the specificity of
421 the response to looming (**Fig. 6A and A'**). Neurons exposed to the looming object
422 continuously increased their firing rate as the object increased in size, followed by a
423 decrease of the firing rate when the object no longer increased in size. A small OFF

424 response can be observed (**Fig. 6B and 6C)**. Neurons exposed to the static object, on
425 the other hand, showed a typical ON-OFF response (**Fig. 6B' and 6C'**). Of a total of 251
426 responsive neurons, 146 responded to both stimuli, 58 only to looming, and 47 only to the
427 static object. Interestingly, the onset time of the response to both stimuli did not differ
428 significantly (paired *t*-test, $p = 0.3$), showing that neurons start their response at the same
429 time irrespective of the visual object shown (**Fig. 7A**). The difference between the
430 response to the looming and to the static object can be observed in other parameters- in
431 peak time (**Fig. 7B**) and maximal firing rate after the initial response (**Fig. 7D**). With the
432 looming parameters used, neurons exposed to the looming take longer to reach their
433 maximal response (paired *t*-test, $p = 0.0066$) and show significantly higher firing rates
434 (paired *t*-test, $p < 0.0016$) than when exposed to the static object.

435

436 **DISCUSSION**

437 It is well known that mature visual properties as well as visual system development differ between
438 mammalian species in a way that is related to the role played by vision in their behavior.
439 Interestingly, most of the recent publications about visual system development and function come
440 from a single model species, the lab mouse *(Mus musculus)*. Lab mice are altricial, nocturnal, and
441 feature a poorly developed visual system when compared with diurnal rodents such as squirrels,
442 guinea pigs and some other New World rodents. Thus, mouse-centered studies may have biased
443 the current understanding of rodent visual system function and its development. As a starting
444 point to counterbalance this bias, we characterized the visual properties of SC neurons in the
445 adult *Octodon degus* in the present study. Degus, contrary to mice and other typical lab rodent
446 species such as rats and hamsters, are diurnal (Fulk 1976) and precocial (Reynolds and Wright

1979; Long and Ebensperger 2010). Furthermore, degus represent a phylogenetic group (suborder Hystricomorpha) apart from old world rodents such as rats and mice (suborder Myomorpha) or squirrels (suborder Sciuromorpha). As we predicted, we found that *O. degus'* SC is a well-developed visual structure, featuring visual properties comparable to that of highly visual rodents such as squirrels (Van Hooser *et al.* 2003) and gerbils (Baker and Emerson 1983). We conclude that, given its precocial and diurnal habit, *O. degus* is especially well-suited as an animal model for studies of visual system development.

Cytoarchitecture of the superior colliculus in *Octodon degus*

Our anatomical results readily confirmed that degus' SC features a laminar differentiation comparable to that of other diurnal mammals, such as the squirrel (Major *et al.* 2003; Fredes *et al.* 2012). In particular, the extensive laminar differentiation of the SGI suggests that in degus the SC serves a stronger and more complex visuomotor role than in other rodents, a conjecture worthy of further studies. In addition, the results of our retinal injections confirm previous studies (Vega-Zuniga et al., 2013; Deichler et al., 2019; 2020) reporting that degu SC receives massive and highly ordered retinal projections. As in the previous studies, we found that retinal afferents enter the contralateral SC through the SO to form dense terminal domains in the stratum griseum superficiale (SGS) and stratum zonale (SZ), and sparser arborizations in the stratum opticum (SO). As expected from studies of other species, retinal projections were not present in the deeper layers of the SC (dSC), namely the stratum griseum intermediale (SGI) and the stratum griseum profundus (SGP).

469 **Receptive field size**

470 We found that the degu's SC has a laminar segregation of RF sizes, with smaller RFs located in
471 superficial layers, and larger RFs in deeper layers. This seems to be a canonical property of the
472 SC -*aka* optic tectum- across vertebrate taxa, in that it has been reported not only in other rodents,
473 such as mice, rats and hamsters (Humphrey 1968; Rhoades and Chalupa 1976; Ito *et al.* 2017),
474 but also in Carnivore species (cats and ferrets; Brecht et al., 1999; Stitt et al., 2013), primates
475 (Humphrey 1968; Cynader and Berman 1972) and birds (Knudsen 1982; Marín *et al.* 2005). This
476 change in RF size across layers correlates with the different morphological characteristics of
477 neurons located in each layer. In mammals, narrow field and stellate neurons located in the upper
478 SGS (uSGS) have narrow dendritic trees and small RFs (Mooney *et al.* 1985; May 2006; Hoy *et*
479 *al.* 2019), whereas wide field and horizontal cells, located in the deeper SGS (dSGS), have large
480 dendritic trees (~500-800 μm) along with very large RFs (~300-1000 deg^2) (Major *et al.* 2000;
481 Fredes *et al.* 2012; Gale and Murphy 2014). In the dSC (SGI and SGP), neurons that have large
482 dendritic trees also exhibit large RFs, most of them being premotor neurons that receive
483 convergent inputs from neurons located in the superficial layers (Isa and Hall 2009).

484 Superior colliculus RF sizes are highly variable across rodent species. In hamsters the SGS
485 RFs are quite large (ranging from 169 deg^2 to ~295 deg^2 [19.4 ± 0.56° diameter] (Carrasco *et al.*
486 2005; Balmer and Pallas 2015). In mice, on the other hand, contrasting results have been
487 reported. Some studies report large RF sizes (average 165 ± 21 deg^2 (Chandrasekaran *et al.*
488 2005; Ito *et al.* 2017) but others report smaller values (107.5 ± 14.9 deg^2, (Wang *et al.* 2010)).
489 These differences may depend on the visual stimulation method used. Ito *et al*. (2017) used a 10º
490 flashing-spot but Wang *et al.* (2010) used a 5º flashing square. In the present study we used a
491 small (3º), moving bright square as a visual stimulus, which is bigger than that used in previous

492 studies of hamsters (1º) (Carrasco *et al.* 2005; Mudd *et al.* 2019). Nevertheless, despite
493 methodological differences, degus seem to have the smallest RF sizes reported in rodents for the
494 sSC so far, with area sizes that never surpassed 100 deg^2 (ranging from 19.8 deg^2 to 74.4 deg^2).
495 It is noteworthy that degus are diurnal animals and possess a cone-rich retina (Chávez *et al.*
496 2003; Jacobs *et al.* 2003; Vega-Zuniga *et al.* 2013). These features suggest that degus would
497 have a visual acuity higher than that of nocturnal species. The comparatively small size of
498 degu SC receptive fields is indeed consistent with a greater visual acuity, reflecting the diurnal
499 specialization of the visual system in these rodents.

500

501 **Response to grating stimuli**

502 In cats, hooded rats, and squirrels, it has been shown that the presence of visual neurons tuned
503 to high spatial frequencies correlates with higher visual acuity (Dean 1981; Issa *et al.* 2000;
504 Heimel *et al.* 2005). In the case of degus, we found that most sSC neurons (> 50%) that responded
505 to gratings exhibited preferences for low/medium spatial frequencies. Interestingly, we found
506 another set of neurons (15%) that were tuned to higher SFs (with a peak of 0.24 cpd). Overall,
507 the SF tuning reported for mouse SC [peak=0.08 cpd, (Wang *et al.* 2010); median= 0.052 cpd,
508 (De Franceschi and Solomon 2018) is lower than what we found in degus, suggesting that, as
509 expected from its diurnal visual specialization, degus have a higher visual acuity than mice.
510 Interestingly, it has been reported that awake mice show an approximately 2-fold higher SF tuning
511 than anesthetized mice (De Franceschi and Solomon 2018)]. Here we only tested deeply
512 anesthetized animals, thus awake degus might show higher SF tuning than we report here.

513

514 *Spatial frequency modulation.* In degu sSC, most (86%) of the neurons recorded exhibited non-
515 linear (F1/F0 <1) responses to grating stimuli, thus showing low modulation by the SF presented.
516 However, some neurons (14%) were modulated by the SF (F1/F0 >1). A similar distribution of
517 linear and non-linear neurons was found in mice (Wang *et al.* 2010). Interestingly, neurons
518 showing low or no SF modulation were tuned to higher frequencies, a phenomenon also reported
519 in mice (De Franceschi and Solomon 2018).

520

521 *Contrast sensitivity.* We found that almost half (44%) of the neurons responded in a linear,
522 monotonically increasing fashion to increasing stimulus contrast (C_{50} > 45), whereas others
523 showed highly or moderately saturating responses to contrast. It has been proposed that
524 saturated responses to contrast, rather than being the result of biophysical limitations of neurons,
525 are due to an active mechanism controlling the gain of contrast responses (Peirce 2007). Thus,
526 saturating responses to contrast relate to higher sensitivity to subtle contrast differences at low
527 contrast values, which is an important adaptation for active nocturnal vision. In mice most SC
528 neurons exhibit non-linear, saturating responses to contrasts (De Franceschi and Solomon 2018),
529 as expected for nocturnal species. Unlike what has been observed in mice, we found no clear
530 bias toward saturating responses to contrast in the degus' SC, likely reflecting the diurnal
531 adaptations of their visual system.

532

533 **Looming responses**

534 In degus, we found many sSC neurons that showed a progressive increase in their responses to
535 an expanding dark disc that simulated a dark looming stimulus approaching against a lighter

536 background. This is similar to what has been reported in mice and hamsters, in which neurons
537 located in sSC respond reliably to repeated presentation of a dark looming stimulus in their RFs
538 (Mudd *et al.* 2019; Lee *et al.* 2020). Most of the neurons recorded in this study (> 55 %) showed
539 a clear difference in their response properties between looming and static stimuli, which reflects
540 the importance of animals responding differentially to different kinds of stimuli, i.e., a fast-
541 approaching object (e.g., a predator) vs. a large, stationary object. In this regard, we observed
542 that neurons responding to both stimulus types (looming and static objects) had significantly
543 higher firing rates when exposed to the looming object than when exposed to the static control,
544 suggesting that the SC possesses a neural mechanism that allows it to identify a fast-approaching
545 object. This mechanism might be involved in the execution of behaviors in this context. In rodents,
546 looming stimuli have been reported to unleash behaviors modulated by SC such as escaping and
547 freezing (Yilmaz and Meister 2013; De Franceschi and Solomon 2018). In degus, looming stimuli
548 projected from the upper, binocular portion of the visual field elicit escape behavior, which is
549 thought to be triggered by the SC/parabigeminal nucleus interaction (Deichler *et al.* 2020).

550

551 **Conclusion**

552 Degus show remarkably specialized visual properties in the superior colliculus compared to
553 commonly studied lab rodents. Our results suggest that degus have diurnal visual characteristics,
554 and a higher visual acuity than other lab rodents. Moreover, degus are precocial, diurnal and
555 belong to a separate clade within the Rodentia order, allowing studies to address from a
556 comparative perspective which visual features are conserved among rodents or other mammals,
557 and which might be determined by their ecological niche. Altogether, we strongly argue that degus
558 are a promising model to study the visual system in general and its development in particular.

BIBLIOGRAPHY

Albano JE, Norton TT, Hall WC (1979) Laminar origin of projections from the superficial layers of the superior colliculus in the tree shrew, *Tupaia glis*. Brain Res 173 (1): 1-11. doi: https://doi.org/10.1016/0006-8993(79)91090-4

Alitto HJ, Rathbun DL, Fisher TG, Alexander PC, Usrey WM (2019) Contrast gain control and retinogeniculate communication. Eur J Neurosci 49 (8): 1061-1068. doi: https://doi.org/10.1111/ejn.13904

Baker AG, Emerson VF (1983) Grating acuity of the mongolian gerbil (*Meriones unguiculatus*). Behav Brain Res 8 (2): 195-209. doi: https://doi.org/10.1016/0166-4328(83)90054-2

Balaram P, Hackett TA, Kaas JH (2011) VGLUT1 mRNA and protein expression in the visual system of prosimian galagos (*Otolemur garnetti*). Eye Brain 3: 81-98. doi: https://doi.org/10.2147/EB.S23007

Balmer TS, Pallas SL (2015) Refinement but not maintenance of visual receptive fields is independent of visual experience. Cereb Cortex 25 (4): 904-917. doi: https://doi.org/10.1093/cercor/bht281

Basso MA, May PJ (2017) Circuits for action and cognition: A view from the Superior Colliculus. Annu Rev Vis 3 (1): 197-226. doi: https://doi.org/10.1146/annurev-vision-102016-061234

Biffi E, Ghezzi D, Pedrocchi A, Ferrigno G (2010) Development and validation of a spike detection and classification algorithm aimed at implementation on hardware devices. Comput Intell Neurosci 2010: Article ID 659050, 15 pages, 2010. doi: https://doi.org/10.1155/2010/659050I

Brainard MS, Doupe AJ (2013) Translating birdsong: songbirds as a model for basic and applied medical research. Annu Rev Neurosci 36: 489-517. doi: https://doi.org/10.1146/annurev-neuro-060909-152826

Camillo D, Ahmadlou M, Heimel JA (2020) Contrast-dependence of temporal frequency tuning in mouse V1. Front Neurosci 14: 868. doi: https://doi.org/10.3389/fnins.2020.00868

Carrasco MM, Pallas SL (2006) Early visual experience prevents but cannot reverse deprivation-induced loss of refinement in adult superior colliculus. Vis Neurosci 23 (6): 845-852. doi: https://doi.org/10.1017/S0952523806230177

Carrasco MM, Razak KA, Pallas SL (2005) Visual experience is necessary for maintenance but not development of receptive fields in superior colliculus. J Neurophysiol 94 (3): 1962-1970. doi: https://doi.org/10.1152/jn.00166.2005

Chandrasekaran A, R. , Plas D, T. , Gonzalez E, Crair M, C. (2005) Evidence for an instructive role of retinal activity in retinotopic map refinement in the superior colliculus of the mouse. J Neurosci 25 (29): 6929-6938. doi: https://doi.org/10.1523/JNEUROSCI.1470-05.2005

Chávez AsE, Bozinovic F, Peichl L, Palacios AnG (2003) Retinal spectral sensitivity, fur coloration, and urine reflectance in the genus *Octodon* (rodentia): Implications for visual ecology. Invest Ophthalmol Vis Sci 44 (5): 2290-2296. doi: https://doi.org/10.1167/iovs.02-0670

603 Choi JH, Jung HK, Kim T (2006) A new action potential detector using the MTEO and its
604 effects on spike sorting systems at low signal-to-noise ratios. IEEE Trans Biomed
605 Eng 53 (4): 738-746. doi: https://doi.org/10.1109/TBME.2006.870239
606 Cynader M, Berman N (1972) Receptive-field organization of monkey superior
607 colliculus. J Neurophysiol 35 (2): 187-201. doi:
608 https://doi.org/10.1152/jn.1972.35.2.187

609

610 De Franceschi G, Solomon SG (2018) Visual response properties of neurons in the
611 superficial layers of the superior colliculus of awake mouse. J Physiol 596 (24):
612 6307-6332. doi: https://doi.org/10.1113/JP276964
613 De Valois RL, Albrecht DG, Thorell LG (1982) Spatial frequency selectivity of cells in
614 macaque visual cortex. Vision Res 22 (5): 545-559. doi:
615 https://doi.org/10.1016/0042-6989(82)90113-4
616 Dean P (1981) Visual pathways and acuity in hooded rats. Behav Brain Res 3 (2): 239-
617 271. doi: https://doi.org/10.1016/0166-4328(81)90050-4
618 DeBello WM, Knudsen EI (2004) Multiple sites of adaptive plasticity in the owl's auditory
619 localization pathway. J Neurosci 24 (31): 6853-6861. doi:
620 https://doi.org/10.1523/jneurosci.0480-04.2004
621 Deichler A, Carrasco D, Gonzalez-Cabrera C, Letelier JC, Marín G, Mpodozis J (2019)
622 The nucleus pretectalis principalis: A pretectal structure hidden in the mammalian
623 thalamus. J Comp Neurol 527 (2): 372-391. doi:
624 https://doi.org/10.1002/cne.24540
625 Deichler A, Carrasco D, Lopez-Jury L, Vega-Zuniga T, Márquez N, Mpodozis J, Marín
626 GJ (2020) A specialized reciprocal connectivity suggests a link between the
627 mechanisms by which the superior colliculus and parabigeminal nucleus produce
628 defensive behaviors in rodents. Sci Rep 10 (1): 16220. doi:
629 https://doi.org/10.1038/s41598-020-72848-0
630 Espinosa JS, Stryker Michael P (2012) Development and plasticity of the primary visual
631 cortex. Neuron 75 (2): 230-249. doi: https://doi.org/10.1016/j.neuron.2012.06.009
632 Fredes F, Vega-Zuniga T, Karten H, Mpodozis J (2012) Bilateral and ipsilateral
633 ascending tectopulvinar pathways in mammals: A study in the squirrel
634 (*Spermophilus beecheyi*). J Comp Neurol 520 (8): 1800-1818. doi:
635 https://doi.org/10.1002/cne.23014
636 Fulk G (1976) Notes on the activity, reproduction and social behaviour of *Octodon*
637 *degus.* J of Mammalogy 57: 495-505. doi: https://doi.org/10.2307/1379298
638 Gale SD, Murphy GJ (2014) Distinct representation and distribution of visual information
639 by specific cell types in mouse superficial superior colliculus. J Neurosci 34 (40):
640 13458-13471. doi: https://doi.org/10.1523/jneurosci.2768-14.2014
641 Garrett ME, Nauhaus I, Marshel JH, Callaway EM (2014) Topography and areal
642 organization of mouse visual cortex. J Neurosci 34 (37): 12587-12600. doi:
643 https://doi.org/10.1523/jneurosci.1124-14.2014
644 Heimel JA, Van Hooser SD, Nelson SB (2005) Laminar organization of response
645 properties in primary visual cortex of the gray squirrel (*Sciurus carolinensis*). J
646 Neurophysiol 94 (5): 3538-3554. doi: https://doi.org/10.1152/jn.00106.2005

647 Helms MC, Özen G, Hall WC (2004) Organization of the intermediate gray layer of the
648 superior colliculus. I. Intrinsic vertical connections. J Neurophysiol 91 (4): 1706-
649 1715. doi: https://doi.org/10.1152/jn.00705.2003
650 Hendrikje N, Andrea H, Ian N, Hiroki T, Huang ZJ, Edward MC (2013) Contrast
651 dependence and differential contributions from somatostatin- and parvalbumin-
652 expressing neurons to spatial integration in mouse V1. J Neurosci 33 (27):
653 11145-11154. doi: https://doi.org/10.1523/jneurosci.5320-12.2013
654 Hensch TK, Fagiolini M, Mataga N, Stryker MP, Baekkeskov S, Kash SF (1998) Local
655 GABA circuit control of experience-dependent plasticity in developing visual
656 cortex. Science 282 (5393): 1504-1508. doi:
657 https://doi.org/10.1126/science.282.5393.1504
658 Hoy JL, Bishop HI, Niell CM (2019) Defined cell types in superior colliculus make
659 distinct contributions to prey capture behavior in the mouse. Curr Biol 29 (23):
660 4130-4138. doi: https://doi.org/10.1016/j.cub.2019.10.017
661 Hubel DH, Wiesel TN (1998) Early exploration of the visual cortex. Neuron 20 (3): 401-
662 412. doi: https://doi.org/10.1016/s0896-6273(00)80984-8
663 Huberman AD, Niell CM (2011) What can mice tell us about how vision works? Trends
664 Neurosci 34 (9): 464-473. doi: https://doi.org/10.1016/j.tins.2011.07.002
665 Humphrey NK (1968) Responses to visual stimuli of units in the superior colliculus of
666 rats and monkeys. Exp Neurol 20 (3): 312-340. doi: https://doi.org/10.1016/0014-
667 4886(68)90076-9
668 Isa T, Hall WC (2009) Exploring the superior colliculus *in vitro*. J Neurophysiol 102 (5):
669 2581-2593. doi: https://doi.org/10.1152/jn.00498.2009
670 Issa NP, Trepel C, Stryker MP (2000) Spatial frequency maps in cat visual cortex. J
671 Neurosci 20 (22): 8504-8514. doi: https://doi.org/10.1523/jneurosci.20-22-
672 08504.2000
673 Ito S, Feldheim DA (2018) The mouse superior colliculus: An emerging model for
674 studying circuit formation and function. Front Neural Circuits 12: 10. doi:
675 https://doi.org/10.3389/fncir.2018.00010
676 Ito S, Feldheim DA, Litke AM (2017) Segregation of visual response properties in the
677 mouse superior colliculus and their modulation during locomotion. J Neurosci 37
678 (35): 8428-8443. doi: https://doi.org/10.1523/jneurosci.3689-16.2017
679 Jacobs GH, Calderone JB, Fenwick JA, Krogh K, Williams GA (2003) Visual
680 adaptations in a diurnal rodent, Octodon degus. J Comp Physiol A 189 (5): 347-
681 361. doi: https://doi.org/10.1007/s00359-003-0408-0
682 Jassik-Gerschenfeld D, Hardy O (1979) Single-neuron responses to moving sine-wave
683 gratings in the pigeon optic tectum. Vision Res 19 (9): 993-999. doi:
684 https://doi.org/10.1016/0042-6989(79)90224-4
685 Jones HG, Brown AD, Koka K, Thornton JL, Tollin DJ (2015) Sound frequency-invariant
686 neural coding of a frequency-dependent cue to sound source location. J
687 Neurophysiol 114 (1): 531-539. doi: https://doi.org/10.1152/jn.00062.2015
688 Juavinett Ashley L, Callaway Edward M (2015) Pattern and component motion
689 responses in mouse visual cortical areas. Curr Biol 25 (13): 1759-1764. doi:
690 https://doi.org/10.1016/j.cub.2015.05.028

Knudsen EI (1982) Auditory and visual maps of space in the optic tectum of the owl. J Neurosci 2 (9): 1177-1194. doi: https://doi.org/10.1523/jneurosci.02-09-01177.1982

Lee KH, Tran A, Turan Z, Meister M (2020) The sifting of visual information in the superior colliculus. eLife 9: e50678. doi: https://doi.org/10.7554/eLife.50678

Letelier JC, Weber PP (2000) Spike sorting based on discrete wavelet transform coefficients. J Neurosci Methods 101 (2): 93-106. doi: https://doi.org/10.1016/S0165-0270(00)00250-8

Long CV, Ebensperger LA (2010) Pup growth rates and breeding female weight changes in two populations of captive bred degus (*Octodon degus*), a precocial caviomorph rodent. Reprod Domest Anim 45 (6): 975-982. doi: https://doi.org/10.1111/j.1439-0531.2009.01470.x

Major DE, Luksch H, Karten HJ (2000) Bottlebrush dendritic endings and large dendritic fields: Motion-detecting neurons in the mammalian tectum. J Comp Neurol 423 (2): 243-260. doi: https://doi.org/10.1002/1096-9861(20000724)423:2<243::AID-CNE5>3.0.CO;2-5

Major DE, Rodman HR, Libedinsky C, Karten HJ (2003) Pattern of retinal projections in the California ground squirrel (*Spermophilus beecheyi*): Anterograde tracing study using cholera toxin. J Comp Neurol 463: 317-340. doi: https://doi.org/10.1002/cne.10764

Marín G, Mpdozis J, Sentis E, Ossandón T, Letelier JC (2005) Oscillatory bursts in the optic tectum of birds represent re-entrant signals from the nucleus isthmi pars parvocellularis. J Neurosci 25 (30): 7081-7089. doi: https://doi.org/10.1523/jneurosci.1379-05.2005

Márquez N, Martínez-Harms J, Vásquez RA, Mpodozis J (2015) Early olfactory environment influences social behaviour in adult *Octodon degus*. PLOS ONE 10 (2): e0118018. doi: https://doi.org/10.1371/journal.pone.0118018

May PJ (2006) The mammalian superior colliculus: laminar structure and connections. Prog Brain Res 151: 321-378. doi: https://doi.org/10.1016/S0079-6123(05)51011-2

Mooney RD, Klein BG, Rhoades RW (1985) Correlations between the structural and functional characteristics of neurons in the superficial laminae and the hamster's superior colliculus. J Neurosci 5 (11): 2989-3009. doi: https://doi.org/10.1523/jneurosci.05-11-02989.1985

Mudd DB, Balmer TS, Kim SY, Machhour N, Pallas SL (2019) Trkb activation during a critical period mimics the protective effects of early visual experience on perception and the stability of receptive fields in adult superior colliculus. J Neurosci 39 (23): 4475-4488. doi: https://doi.org/10.1523/jneurosci.2598-18.2019

Naka KI, Rushton WA (1966) S-potentials from colour units in the retina of fish (Cyprinidae). J Physiol 185 (3): 536-555. doi: https://doi.org/10.1113/jphysiol.1966.sp008001

Niell CM, Stryker MP (2008) Highly selective receptive fields in mouse visual cortex. J Neurosci 28 (30): 7520-7536. doi: https://doi.org/10.1523/jneurosci.0623-08.2008

Peirce JW (2007) The potential importance of saturating and supersaturating contrast response functions in visual cortex. J Vis 7 (6): 1-10. doi: https://doi.org/10.1167/7.6.13

Razak KA (2011) Systematic representation of sound locations in the primary auditory cortex. J Neurosci 31 (39): 13848-13859. doi: https://doi.org/10.1523/jneurosci.1937-11.2011

Razak KA, Fuzessery ZM (2015) Development of echolocation calls and neural selectivity for echolocation calls in the pallid bat. Dev Neurobiol 75 (10): 1125-1139. doi: https://doi.org/10.1002/dneu.22226

Reynolds TJ, Wright JW (1979) Early postnatal physical and behavioural development of degus (*Octodon degus*). Lab Anim 13 (2): 93-100. doi: https://doi.org/10.1258/002367779780943576

Rhoades RW, Chalupa LM (1976) Directional selectivity in the superior colliculus of the golden hamster. Brain Res 118 (2): 334-338. doi: https://doi.org/10.1016/0006-8993(76)90721-6

Rousseeuw PJ (1987) Silhouettes: A graphical aid to the interpretation and validation of cluster analysis. J Comput Appl Math 20: 53-65. doi: https://doi.org/10.1016/0377-0427(87)90125-7

Van Hooser SD, Heimel JAF, Nelson SB (2003) Receptive field properties and laminar organization of lateral geniculate nucleus in the gray squirrel (*Sciurus carolinensis*). J Neurophysiol 90 (5): 3398-3418. doi: https://doi.org/10.1152/jn.00474.2003

Vega-Zuniga T, Medina FS, Fredes F, Zuniga C, Severín D, Palacios AG, Karten HJ, Mpodozis J (2013) Does nocturnality drive binocular vision? Octodontine rodents as a case study. PLOS ONE 8 (12): e84199. doi: https://doi.org/10.1371/journal.pone.0084199

Wang L, Sarnaik R, Rangarajan K, Liu X, Cang J (2010) Visual receptive field properties of neurons in the superficial superior colliculus of the mouse. J Neurosci 30 (49): 16573-16584. doi: https://doi.org/10.1523/jneurosci.3305-10.2010

Wiener SI (1986) Laminar distribution and patchiness of cytochrome oxidase in mouse superior colliculus. J Comp Neurol 244 (2): 137-148. doi: https://doi.org/10.1002/cne.902440202

Yilmaz M, Meister M (2013) Rapid innate defensive responses of mice to looming visual stimuli. Curr Biol 23 (20): 2011-2015. doi: https://doi.org/10.1016/j.cub.2013.08.015

771 **TABLES**

772 **Table 1.**

Depth range (µm)*	SC layer	Depth range
< 400	SGS	1
(400, 500)	SGS	2
(501, 600)	SO	3
(601, 750)	SO	4
(751, 950)	SGI	5
(951, 1100)	SGI	6
(1101, 1300)	SGI	7

773

774 **Table 1. Categorization of depth ranges.** Visual responses were systematically
775 recorded from neurons with RFs located within the frontal visual field, at intervals of 100
776 µm along transects across the SC layers. Neuronal responses were categorized into
777 seven distinct depth ranges according to the depth at which they were recorded.

778

779

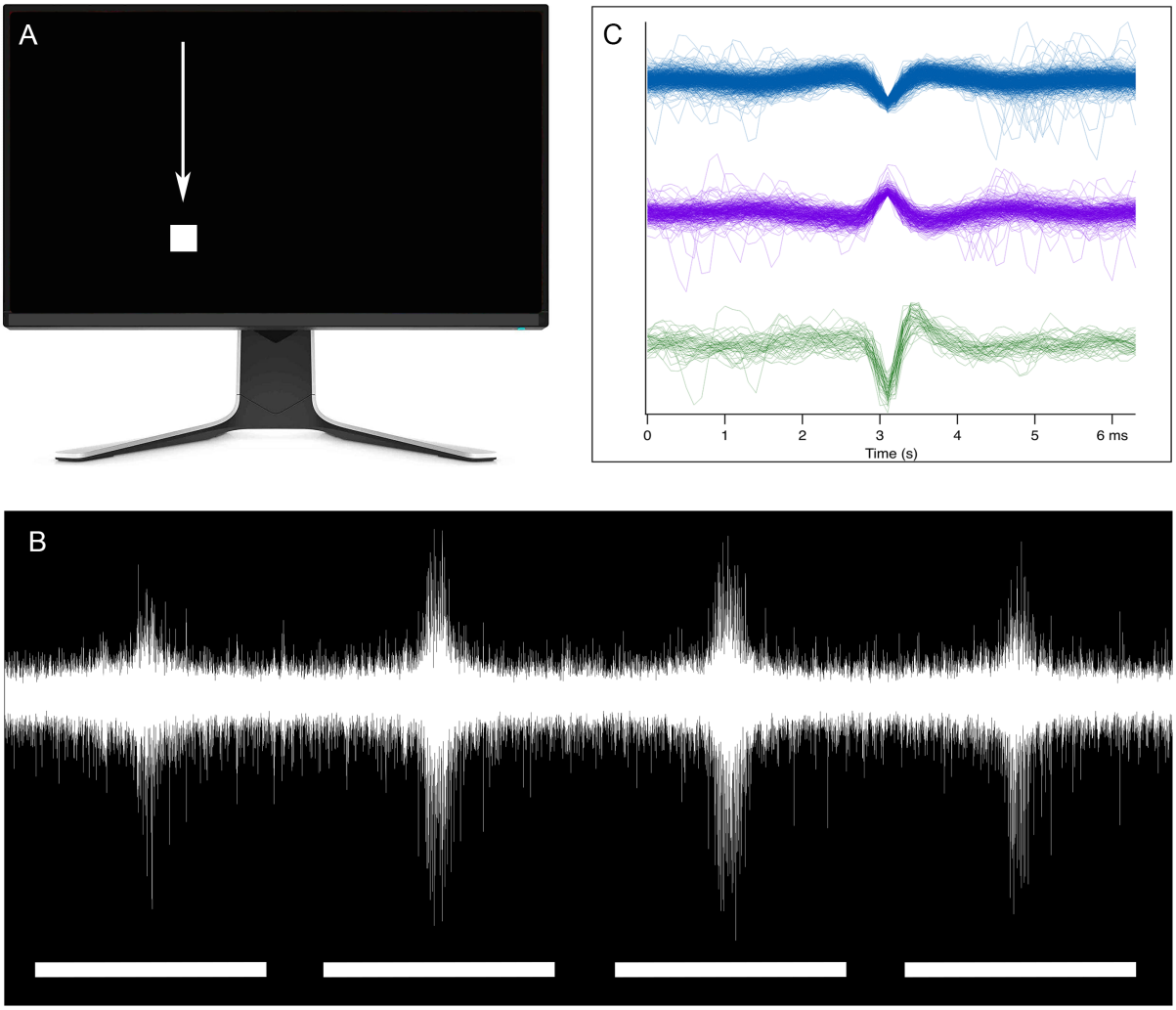

Figure 1. Visual stimulation, extracellular recording, and spike sorting. (A) Visual stimuli used to characterize RF size and shape. A small white square (~3° diameter) on a black background was swept across the screen monitor from top to bottom with each vertical sweep (27°/s, 4 sec), displaced horizontally by 3°, at 1s intervals, to cover the entire screen. (B) Top trace, extracellular responses in the SC. Bottom trace, the visual stimulus on/off pattern as described in A. (C) Example of 3 different single units isolated from recordings.

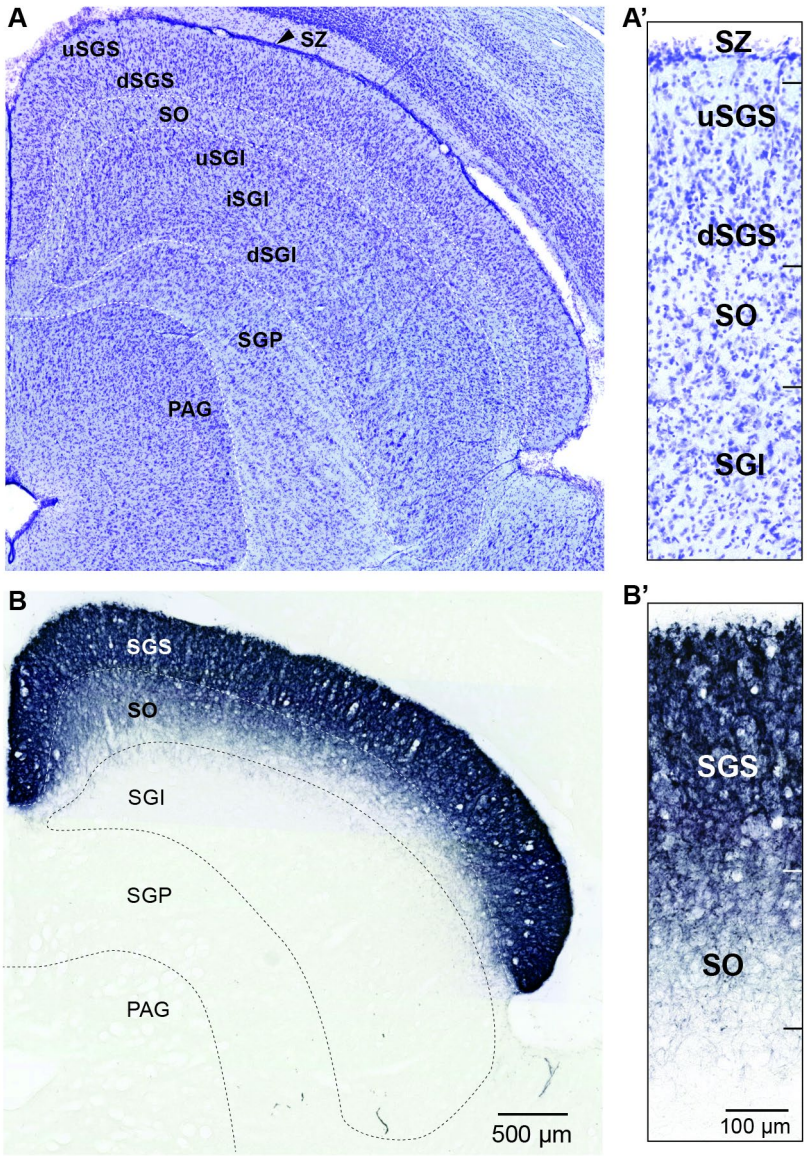

Figure 2. (A) Photomicrograph of a Nissl-stained coronal section showing the subdivisions of the degus' SC: stratum griseum superficiale (SGS) upper (uSGS) and deeper (dSGS), stratum opticum (SO), stratum griseum intermediale (SGI) upper (uSGI), intermediate (iSGI) and deeper (dSGI), the stratum griseum profundus (SGP), and PAG, periacueductal gray. **(A')** Detail of a Nissl-stained coronal section of SC laminae. **(B)** Anterograde labeling of retinotectal projections after a CTB injection into the contralateral eye. **(B')** Detail of the retinotectal projection into the different layers of the degus' SC.

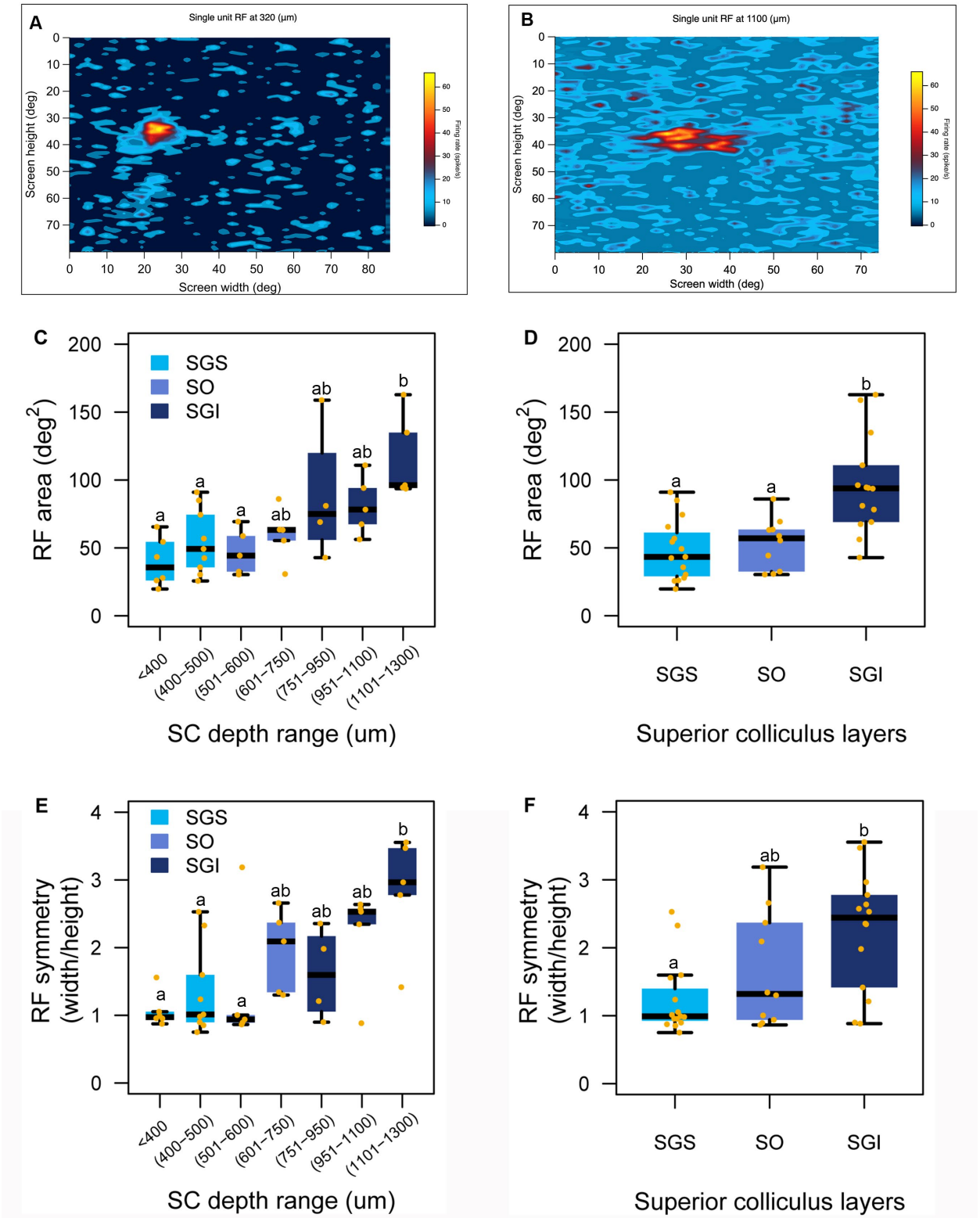
A
Single unit RF at 320 (µm)
Screen height (deg)
Screen width (deg)
Firing rate (spikes/s)
B
Single unit RF at 1100 (µm)
Screen height (deg)
Screen width (deg)
Firing rate (spikes/s)
C
SGS
SO
SGI
RF area (deg^2)
<400
(400–500)
(501–600)
(601–750)
(751–950)
(951–1100)
(1101–1300)
SC depth range (um)
D
RF area (deg^2)
SGS
SO
SGI
Superior colliculus layers
E
SGS
SO
SGI
RF symmetry (width/height)
<400
(400–500)
(501–600)
(601–750)
(751–950)
(951–1100)
(1101–1300)
SC depth range (um)
F
RF symmetry (width/height)
SGS
SO
SGI
Superior colliculus layers

802 **Figure 3. Receptive field size and shape change across SC layers in degus. (A)** Heat
803 map showing the RF of a single unit isolated at 320 µm depth in the SGS mapped by
804 visual stimulation as in Fig. 1A. **(B)** Heat map showing the RF of a unit at 1100 (µm) in
805 the SGI mapped with the same stimulation, at the same recording site (stereotaxic
806 coordinates) as in **A**, but deeper**. (C)** Boxplot of RF areas (in deg^2) across depths ranges
807 from the SGS to the SGI. Boxplots show standard interquartile range (IQR) and median
808 value (black central line), yellow dots are the individual data points. RFs increase in size
809 with depth (ANOVA: $p < 0.01$). **(D)** Boxplot of RF areas across SC layers (SGS, SO and
810 SGI). **(E)** Boxplot of RF shape expressed as the width/height ratio at different SC depth
811 ranges. RFs widen along the horizontal axis with depth (ANOVA: $p < 0.01$). **(F)** Boxplot of
812 RF shape at different SC layers. Different letters above each group in B, C, D, and F
813 represent statistically significant differences (Tukey post-hoc test, see text for exact *p*-
814 values).

815

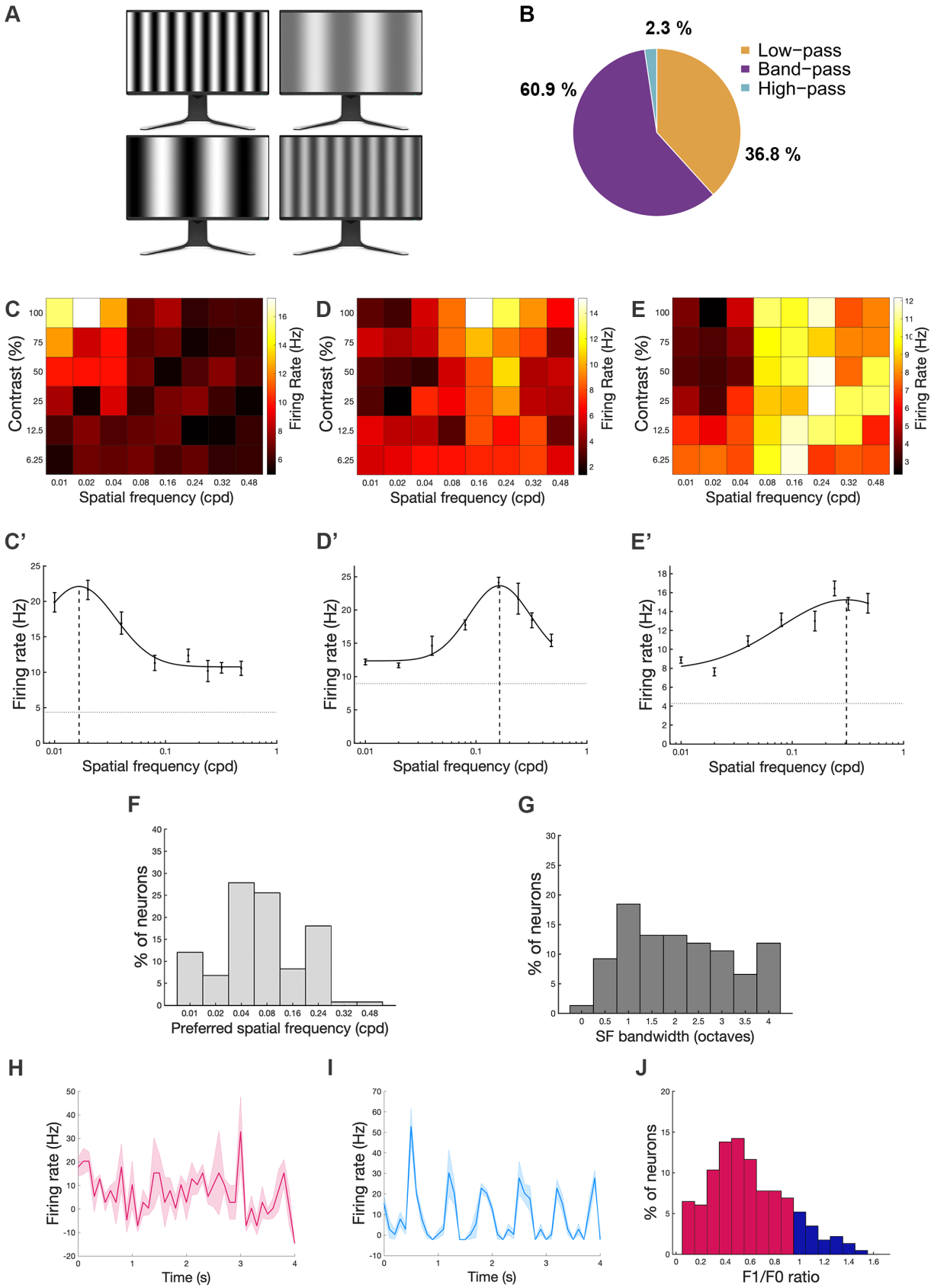
A
B
2.3 %
60.9 %
36.8 %
Low−pass
Band−pass
High−pass
C
D
E
Contrast (%)
Spatial frequency (cpd)
Firing Rate (Hz)
C'
D'
E'
Firing rate (Hz)
F
% of neurons
Preferred spatial frequency (cpd)
G
SF bandwidth (octaves)
H
I
J
Time (s)
F1/F0 ratio

816

817 **Figure 4. Single units show selectivity to spatial frequency.** sSC neurons have a
818 narrow bandwidth, and a small proportion of them (14%) respond linearly to sinusoidal
819 gratings. **(A)** Illustration of the drifting grating stimulus types. Spatial frequency and
820 contrast were varied in a pseudorandom manner. **(B)** Percentage of neurons with low-
821 pass, band-pass or high-pass selectivity to different spatial frequencies (n = 128). **(C-E)**
822 Response matrix (instantaneous firing rate, in Hz) of three different neurons to all contrast
823 and spatial frequency combinations. **(C′-E′)** Examples of low-pass **(C′)**, band-pass **(D′)**,
824 and high pass **(E′)** tuning of the same single neurons as in **C-E**. **(F)** Bar plot of spatial
825 frequency preference for the population. Most units are tuned to 0.04 or 0.08 (cpd), and
826 a smaller group is tuned to higher spatial frequency (0.24 cpd). **(G)** Bar plot of bandwidth
827 showing that most neurons (>50%) are tuned to a certain spatial frequency with narrow
828 bandwidths. **(H-I)** Solid lines are the mean firing rate (100 ms bins) and shaded regions
829 represent mean ± sd. **(H)** Example of a single unit responding non-linearly to 4 seconds
830 of stimulation with a sinusoidal grating (linearity index F1/F0 < 1, where *F1* is the response
831 at the drift frequency, and *F0* is the average firing rate). **(I)** Example of a different single
832 unit responding in a linear manner to sinusoidal gratings (F1/F0 >1). **(J)** Histogram of the
833 linearity index across the entire population of single units (n = 232) showing neurons
834 responding linearly to sinusoidal gratings (red bars) and neurons with non-linear
835 responses to sinusoidal gratings (blue bars).

836

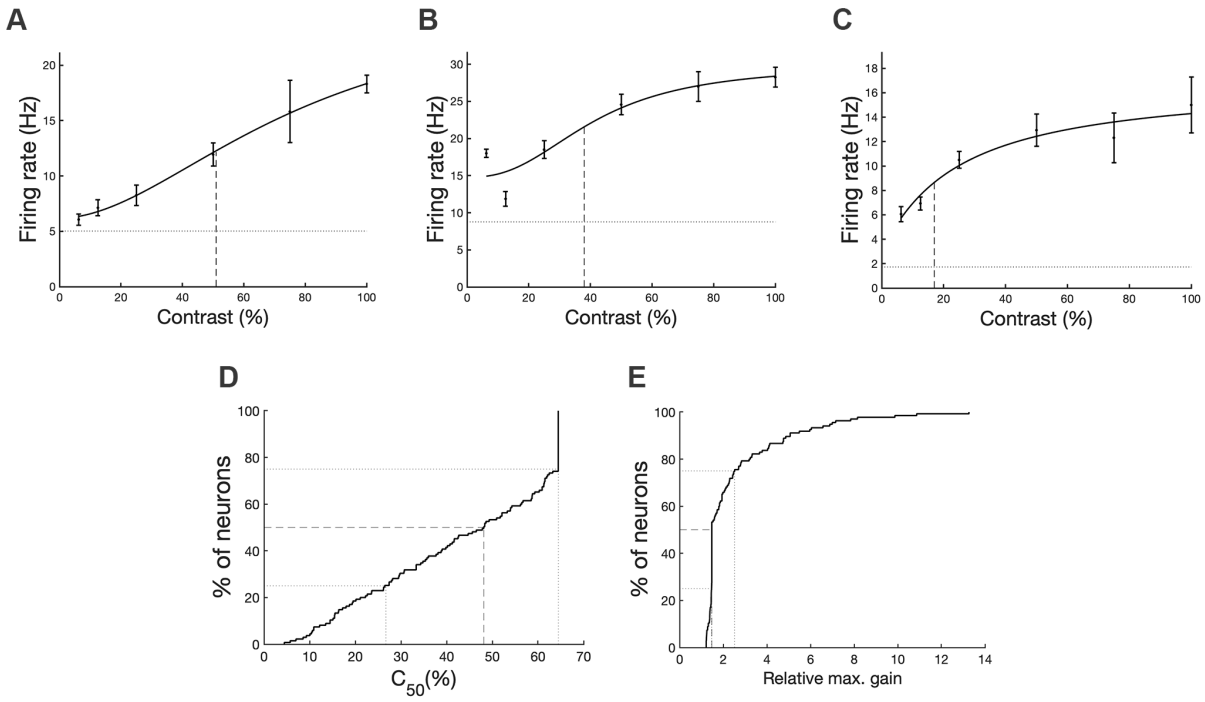

Figure 5. SC Single units show linear or non-linear responses to contrast. Example of three different single units' tuning to contrast, ranging from linear **(A)** to non-linear **(B and C).** All three curves are fitted with a Naka-Rushton function (black line). The dotted line is the spontaneous firing rate (Hz) and the dashed line is the C_{50} (the contrast at half the peak response)**.** Note that **(B)** and **(C)** show saturating responses and differ in their C_{50} values (~40 and ~20, respectively). **(D)** Cumulative histogram of C_{50} distribution (N=135), with the median C_{50} = 48. **(E)** Cumulative histogram (N=135) of the relative maximum gain (see Methods).

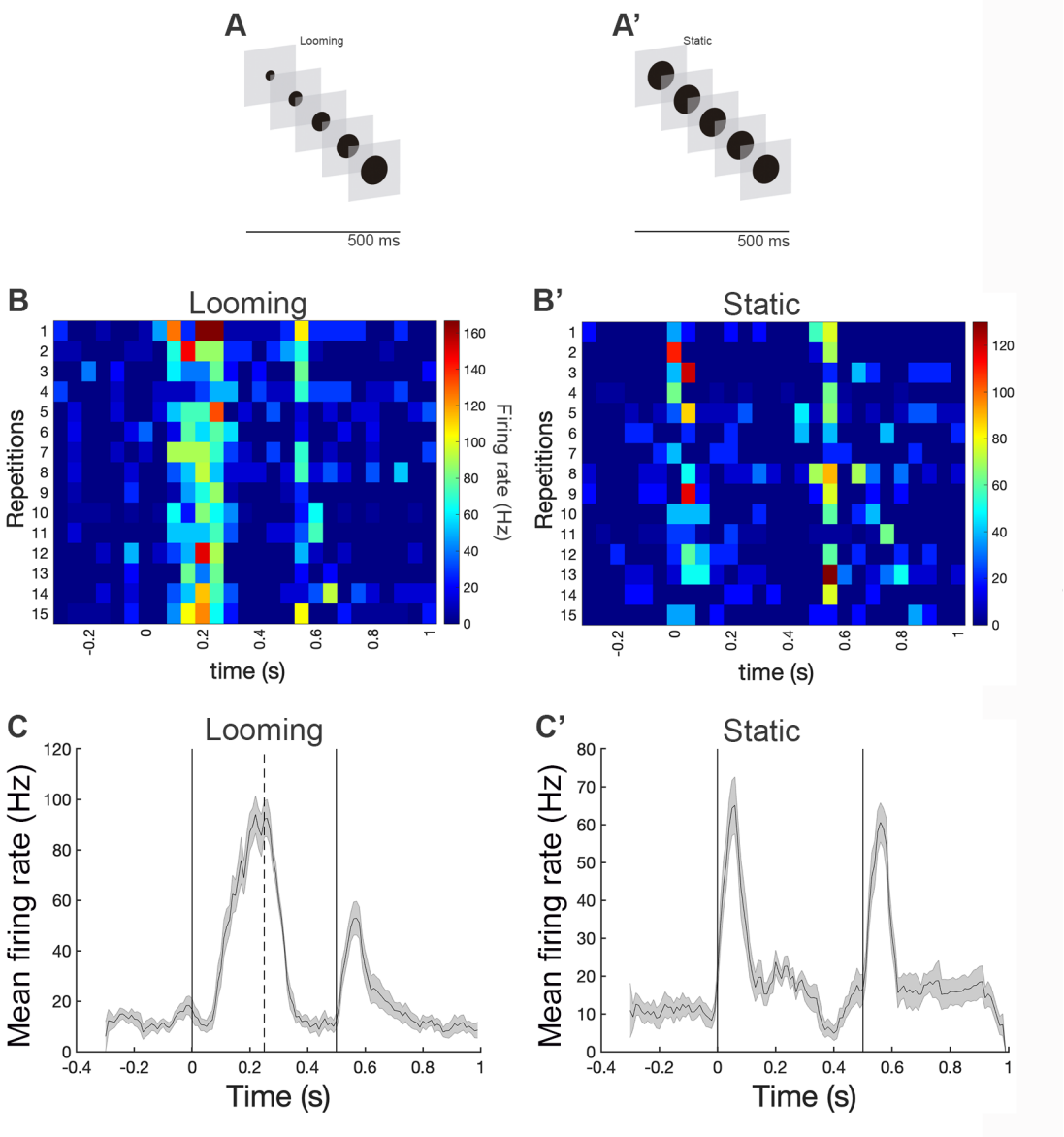

Figure 6. Single units show a continuous buildup of response level to looming stimuli but an ON-OFF response to static stimuli. (A) Diagram of visual stimulation. The looming object increased in size from 2° to 20° over 250 ms, followed by 250 ms at the 20°size. **(A')** The static object was 20° in diameter and was presented for 500 ms. **(B-B')** Heatmap showing instantaneous firing rates of a single unit responding to 15 consecutive presentations of a looming object **(B)** or of a static object **(B'). (C-C')** PSTH

857 of the same single unit showing the mean firing rate for responses to the looming **(C)** and

858 static objects **(C')** across the 15 trials (mean ± SE).

859

860

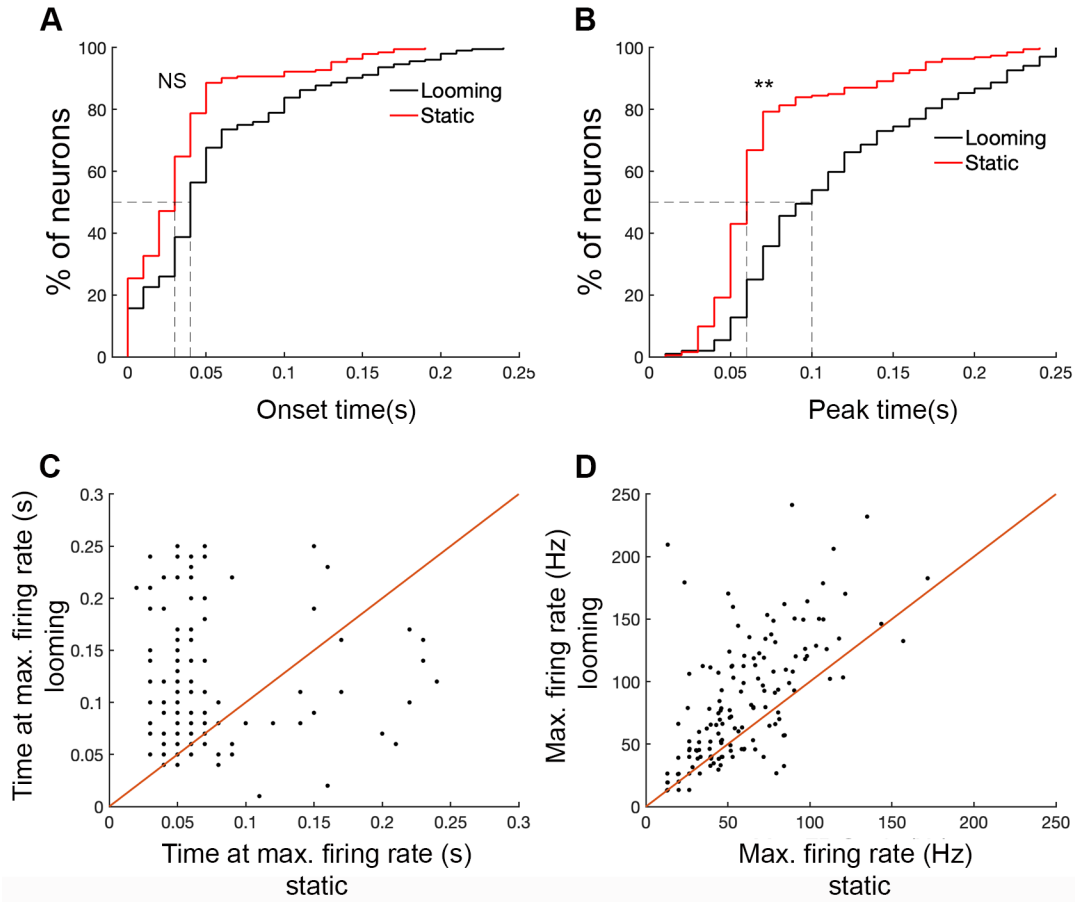

Figure 7. Neurons respond differentially to looming and static objects.

(A) Cumulative probability for onset time comparing both visual stimulus types. Single units responded with similar onset time to both types (static object (red), looming object (black)). **(B)** Cumulative probability for the timing of peak activity comparing responses to looming (black) and static visual stimuli (red). Single units reach their peak activity significantly faster with the static object than with the looming object ($p \geq 0.05$). **(C)** Time at maximal firing rate of neurons responding to both the looming and to the static object; note that most neurons fall above the identity line (slope = 1.0; red) indicating that their maximal firing occurs later in time when exposed to looming compared to the static object.

(D) Maximum firing rate to each visual stimulus of neurons that responded to both stimuli. Interestingly, neurons show higher firing rates when exposed to looming stimuli.

875 **FIGURE LEGENDS**

876 **Figure 1. Visual stimulation, extracellular recording, and spike sorting. (A)** Visual
877 stimuli used to characterize RF size and shape. A small white square (~3° diameter) on
878 a black background was swept across the screen monitor from top to bottom with each
879 vertical sweep (27°/s, 4 sec), displaced horizontally by 3°, at 1s intervals, to cover the
880 entire screen. **(B)** Top trace, extracellular responses in the SC. Bottom trace, the visual
881 stimulus on/off pattern as described in **A**. **(C)** Example of 3 different single units isolated
882 from recordings.

883 **Figure 2. (A)** Photomicrograph of a Nissl-stained coronal section showing the
884 subdivisions of the degus' SC: stratum griseum superficiale (SGS) upper (uSGS) and
885 deeper (dSGS), stratum opticum (SO), stratum griseum intermediale (SGI) upper (uSGI),
886 intermediate (iSGI) and deeper (dSGI), the stratum griseum profundus (SGP), and PAG,
887 periacueductal gray. **(A')** Detail of a Nissl-stained coronal section of SC laminae. **(B)**
888 Anterograde labeling of retinotectal projections after a CTB injection into the contralateral
889 eye. **(B')** Detail of the retinotectal projection into the different layers of the degus' SC.

890

891 **Figure 3. Receptive field size and shape change across SC layers in degus. (A)** Heat
892 map showing the RF of a single unit isolated at 320 µm depth in the SGS mapped by
893 visual stimulation as in Fig. 1A. **(B)** Heat map showing the RF of a unit at 1100 (µm) in
894 the SGI mapped with the same stimulation, at the same recording site (stereotaxic
895 coordinates) as in **A**, but deeper**. (C)** Boxplot of RF areas (in deg^2) across depths ranges
896 from the SGS to the SGI. Boxplots show standard interquartile range (IQR) and median

897 value (black central line), yellow dots are the individual data points. RFs increase in size
898 with depth (ANOVA: $p < 0.01$). **(D)** Boxplot of RF areas across SC layers (SGS, SO and
899 SGI). **(E)** Boxplot of RF shape expressed as the width/height ratio at different SC depth
900 ranges. RFs widen along the horizontal axis with depth (ANOVA: $p < 0.01$). **(F)** Boxplot of
901 RF shape at different SC layers. Different letters above each group in B, C, D, and F
902 represent statistically significant differences (Tukey post-hoc test, see text for exact *p*-
903 values).

904

905 **Figure 4. Single units show selectivity to spatial frequency.** sSC neurons have a
906 narrow bandwidth, and a small proportion of them (14%) respond linearly to sinusoidal
907 gratings. **(A)** Illustration of the drifting grating stimulus types. Spatial frequency and
908 contrast were varied in a pseudorandom manner. **(B)** Percentage of neurons with low-
909 pass, band-pass or high-pass selectivity to different spatial frequencies (n = 128). **(C-E)**
910 Response matrix (instantaneous firing rate, in Hz) of three different neurons to all contrast
911 and spatial frequency combinations. **(C′-E′)** Examples of low-pass **(C′)**, band-pass **(D′)**,
912 and high pass **(E′)** tuning of the same single neurons as in **C-E**. **(F)** Bar plot of spatial
913 frequency preference for the population. Most units are tuned to 0.04 or 0.08 (cpd), and
914 a smaller group is tuned to higher spatial frequency (0.24 cpd). **(G)** Bar plot of bandwidth
915 showing that most neurons (>50%) are tuned to a certain spatial frequency with narrow
916 bandwidths. **(H-I)** Solid lines are the mean firing rate (100 ms bins) and shaded regions
917 represent mean ± sd. **(H)** Example of a single unit responding non-linearly to 4 seconds
918 of stimulation with a sinusoidal grating (linearity index F1/F0 < 1, where *F1* is the response

919 at the drift frequency, and *F0* is the average firing rate). **(I)** Example of a different single
920 unit responding in a linear manner to sinusoidal gratings (F1/F0 >1). **(J)** Histogram of the
921 linearity index across the entire population of single units (n = 232) showing neurons
922 responding linearly to sinusoidal gratings (red bars) and neurons with non-linear
923 responses to sinusoidal gratings (blue bars).

924

925 **Figure 5. SC Single units show linear or non-linear responses to contrast.** Example
926 of three different single units' tuning to contrast, ranging from linear **(A)** to non-linear **(B**
927 **and C).** All three curves are fitted with a Naka-Rushton function (black line). The dotted
928 line is the spontaneous firing rate (Hz) and the dashed line is the C_{50} (the contrast at half
929 the peak response)**.** Note that **(B)** and **(C)** show saturating responses and differ in their
930 C_{50} values (~40 and ~20, respectively). **(D)** Cumulative histogram of C_{50} distribution
931 (N=135), with the median C_{50} = 48. **(E)** Cumulative histogram (N=135) of the relative
932 maximum gain (see Methods).

933 **Figure 6. Single units show a continuous buildup of response level to looming**
934 **stimuli but an ON-OFF response to static stimuli. (A)** Diagram of visual stimulation.
935 The looming object increased in size from 2° to 20° over 250 ms, followed by 250 ms at
936 the 20°size. **(A')** The static object was 20° in diameter and was presented for 500 ms. **(B-**
937 **B')** Heatmap showing instantaneous firing rates of a single unit responding to 15
938 consecutive presentations of a looming object **(B)** or of a static object **(B'). (C-C')** PSTH
939 of the same single unit showing the mean firing rate for responses to the looming **(C)** and
940 static objects **(C')** across the 15 trials (mean ± SE).

941

942 **Figure 7. Neurons respond differentially to looming and static objects.**

943 **(A)** Cumulative probability for onset time comparing both visual stimulus types. Single
944 units responded with similar onset time to both types (static object (red), looming object
945 (black)). **(B)** Cumulative probability for the timing of peak activity comparing responses to
946 looming (black) and static visual stimuli (red). Single units reach their peak activity
947 significantly faster with the static object than with the looming object ($p \geq 0.05$). **(C)** Time
948 at maximal firing rate of neurons responding to both the looming and to the static object;
949 note that most neurons fall above the identity line (slope = 1.0; red) indicating that their
950 maximal firing occurs later in time when exposed to looming compared to the static object.
951 **(D)** Maximum firing rate to each visual stimulus of neurons that responded to both stimuli.
952 Interestingly, neurons show higher firing rates when exposed to looming stimuli.